



## Double pulse laser ablation and laser induced breakdown spectroscopy: A modeling investigation

Annemie Bogaerts\*, Zhaoyang Chen, David Autrique

University of Antwerp, Department of Chemistry, Research Group PLASMANT, Universiteitsplein 1, B-2610 Wilrijk-Antwerp, Belgium

### ARTICLE INFO

#### Article history:

Received 1 February 2008

Accepted 7 April 2008

Available online 20 April 2008

#### Keywords:

Double pulse

Laser ablation

Laser induced breakdown spectroscopy

Numerical modeling

Plume expansion

### ABSTRACT

A numerical model, describing laser–solid interaction (i.e., metal target heating, melting and vaporization), vapor plume expansion, plasma formation and laser–plasma interaction, is applied to describe the effects of double pulse (DP) laser ablation and laser induced breakdown spectroscopy (LIBS). Because the model is limited to plume expansion times in the order of (a few) 100 ns in order to produce realistic results, the interpulse delay times are varied between 10 and 100 ns, and the results are compared to the behavior of a single pulse (SP) with the same total energy. It is found that the surface temperature at the maximum is a bit lower in the DP configuration, because of the lower irradiance of one laser pulse, but it remains high during a longer time, because it rises again upon the second laser pulse. Consequently, the target remains for a longer time in the molten state, which suggests that laser ablation in the DP configuration might be more efficient, through the mechanism of splashing of the molten target. The total laser absorption in the plasma is also calculated to be clearly lower in the DP configuration, so that more laser energy can reach the target and give rise to laser ablation. Finally, it is observed that the plume expansion dynamics is characterized by two separate waves, the first one originating from the first laser pulse, and the second (higher) one as a result of the second laser pulse. Initially, the plasma temperature and electron density are somewhat lower than in the SP case, due to the lower energy of one laser pulse. However, they rise again upon the second laser pulse, and after 200 ns, they are therefore somewhat higher than in the SP case. This is especially true for the longer interpulse delay times, and it is expected that these trends will be continued for longer delay times in the  $\mu$ s-range, which are most typically used in DP LIBS, resulting in more intense emission intensities.

© 2008 Elsevier B.V. All rights reserved.

### 1. Introduction

Laser induced breakdown spectroscopy (LIBS) is a well-known analytical technique for the analysis of solid, liquid, gaseous and aerosol samples (e.g., [1,2]). It suffers, however, from low sensitivity, in comparison with other spectrometric methods [2]. One of the approaches to overcome this limitation is the double (or dual) pulse (DP) configuration (e.g., [3–27]). In this way, the LIBS sensitivity is improved due to a better coupling of the laser energy to the target and ablated material.

Also for laser ablation inductively coupled plasma mass spectrometry (LA-ICP-MS), the DP technique has been applied, by Russo et al., to break the ablated mass into a finer aerosol, which is more readily transported to and digested in the ICP [28]. Moreover, for the application of laser machining of metals, Forsman et al. observed an enhancement of material removal rates when applying the DP technique [29], and Zhang et al. reported high quality laser ablation (i.e., smooth surfaces due to reduced debris deposition) of fused quartz, when applying double pulses with 30 ps–4 ns interpulse delay

times [30]. Finally, for pulsed laser deposition (PLD) the DP technique has proved to be capable for large-area, uniform film growth due to increased plume expansion and higher plasma temperatures [31].

An excellent review paper on the topic of DP LIBS, by Babushok et al., has recently been published in this journal [3]. An overview was given on different configurations, including collinear, orthogonal pre-ablation, orthogonal re-heating and dual pulse crossed beam modes. In addition, the effects of combining laser pulses with different wavelengths (e.g., UV and IR [8]), energies, pulse durations (e.g., femtosecond (fs) and nanosecond (ns) [24]) and interpulse delay times were reviewed. Enhancement effects are reported for a wide variety of parameters, including ion yield, kinetic energy of ions, plasma temperature, plume expansion velocity, size and shape of the plasma volume, emission line intensities,... (see Ref. [3] for a detailed overview). Most often, interpulse delay times in the microsecond range are applied, because this gives most pronounced enhancements in the LIBS emission intensities (e.g., [4–21]). However, enhancements (e.g., for the material ablation rate) were reported also for interpulse delay times in the ns-range or even ps-range, for instance by Russo and coworkers [14,28], as well as other researchers [29–32].

The review paper by Babushok et al. also gives an overview of the possible mechanisms behind the DP effect, both with respect to the

\* Corresponding author.

E-mail address: [annemie.bogaerts@ua.ac.be](mailto:annemie.bogaerts@ua.ac.be) (A. Bogaerts).

ablation processes and the vapor plume/plasma [3]. Furthermore, another recent review paper also discusses the emission enhancement mechanisms in DP LIBS [25]. It is mentioned in this paper that the enhancements are clear, but the mechanisms behind it are still not so well understood. There exist several explanations, depending on the interpulse delay time, such as an increased pulse-plasma coupling (reflected in the higher plasma temperature and electron densities), an increased sample heating, yielding more ablation, and ambient gas rarefaction (see Ref. [25] for more details and corresponding references).

To obtain more insight in these DP effects, several research groups have experimentally investigated the mechanisms of DP LIBS enhancements. Cristoforetti, Tognoni and colleagues have studied the DP effects by spectroscopic analysis, measuring line intensities (emission enhancements), but also electron densities and temperatures in the plume [4–7,19,26] as well as the evolution of the plume by shadowgraphic analysis [6,19]. In Ref. [6] a three-dimensional analysis of the laser-induced plasma was made by spectrally, temporally and spatially resolved measurements and a deconvolution algorithm. Moreover, in Ref. [4] the crater was studied by video-confocal microscopy, and the variation in crater dimensions was correlated to the enhancements in the LIBS signals. Recently, they presented a very interesting spectroscopic study of the factors concurring to intensity enhancements in DP LIBS [26]. This study provided an easy check of the temperature in the plasma. The approach is able to discriminate between the effects of re-heating of the plasma by the second laser pulse, and enhance ablation, and to assess the contribution of these effects to the observed enhancements.

Noll et al. [11] also studied the dynamics of the expanding laser-induced plasma by a high-speed electro-optic camera. A Mach-Zehnder interferometer was applied to detect the spatio-temporal changes of the refractive index of the plasma. The same group measured the material ablation rates, electron density and temperature and line intensities, and reported enhancements for all these quantities when using double pulses [12]. Colao et al. [13] used spectroscopic diagnostics of the plasma to determine the electron densities and plasma temperatures. They observed a lowering in the second pulse-plasma threshold and an overall enhancement in the line emission, for an interpulse delay time of 40–60  $\mu\text{s}$ . Gautier et al. investigated the influence of the interpulse delay time (in the range of 0.2–5  $\mu\text{s}$ ) from temporal and spectral analysis [9,10].

A very interesting study on the effect of interpulse delay time (in the range of 1 ns–10  $\mu\text{s}$ ) was performed by Russo et al. [14]. They observed an abrupt increase in the plasma properties (plasma temperature and electron density) and crater dimensions between 100 and 200 ns, which they attributed to a phase explosion mechanism. Forsman et al. [29] also observed a higher mass removal rate when the interpulse delay time was increased in the range of 30–150 ns, and this was explained by a mechanism of ablation of the target by heated ejecta. The latter were produced by the first laser pulse, and subsequently heated by the second laser pulse.

In general, several authors have reported a reduction in ambient gas density as a result of the first laser pulse, which yields a faster vapor plume expansion (and hence a larger plasma volume) and less effective shielding of the second laser pulse [4–7,9,11,17–19]. The same effect was also observed when varying the ambient gas pressure in single pulse LIBS [5]. Also, the measured increase in the plume temperature in the DP configuration can explain why lines originating from higher excited levels are more enhanced than other lines [4,8,9]. In a very interesting study of enhanced LIBS signals using a combination of 1064 nm and 266 nm laser pulses, St-Onge et al. [8] observed also larger signal enhancements for ionic lines than for atomic lines, which were also correlated with a higher plume temperature. Moreover, the optimum interpulse delay time appeared to be around 100 ns for atomic lines and about 3  $\mu\text{s}$  for ionic lines. A similar observation was made by Cristoforetti et al. [5] and by Gautier et al. [10].

Recently, De Giacomo et al. [27] were able to shed a new light on the expansion dynamics in SP and DP LIBS, by means of spectrally resolved imaging. Based on temporal and spatial maps of the emission signals of atomic and ionic lines, a very interesting information was obtained on the plume expansion dynamics, for instance the recombining character of a SP laser-induced plasma, and the fact that the DP laser-induced plasma expands in a hotter environment, thereby keeping its energy for longer times. This results in a higher ionization degree during longer times and a more stable signal. The spatial and temporal maps of TiI and TiII intensities showed maximum values which were quite similar, but the position and time of the maxima were different, i.e., in the DP case, the maximum was obtained later in time and further away from the target. Hence, in this way the authors could demonstrate that the enhancement is connected to the detection time and the optical configuration. It is concluded that the most important feature of DP LIBS is the possibility to increase the detection time window and the emission volume, thus obtaining a more stable and intense emission signal. This experimental work was complemented by simple modeling of the expansion dynamics (by Euler equations), including the chemical kinetics. The same research group has also applied experimental and modeling techniques to investigate DP LIBS under water [15,16]. The laser-induced bubble, produced by the first pulse, was simulated to clarify the effect of interpulse delay time. It was established that the dynamics of the plasma by DP LIBS was strongly affected by the chemical reactions between the plasma species and the background environment inside the bubble. A hydrodynamic theoretical expansion model was also used in Ref. [31] to yield radial thickness profiles of the deposited films in DP laser deposition.

In our paper, we will try to obtain a deeper understanding of the mechanisms behind DP LIBS, by a more comprehensive model, describing also the laser–solid interaction (ablation), besides plume expansion and plasma formation. Moreover, the plume expansion dynamics is modeled by the full Navier–Stokes equations, taking into account also the interaction terms (viscosity, diffusion, thermal conductivity) between vapor plume and background gas.

## 2. Brief description of the model

The model applied for this study was developed before in our research group [33]. It is a one-dimensional model, describing (i) the laser–metal interaction by a heat conduction equation, yielding heating, melting and vaporization of the metal target, (ii) the vapor plume expansion in a background gas by fluid dynamics equations, including interaction terms between vapor and gas (see above), (iii) the plasma formation, assuming local thermal equilibrium (LTE) conditions, hence using Saha equations to calculate the ionization degree in the vapor and the background gas, and (iv) the laser–plasma interaction by inverse Bremsstrahlung and photo-ionization, resulting in plasma shielding. More details about this model, the input data and the solution methods, can be found in Ref. [33].

The model was already applied to expansion in vacuum [34] and in a background gas with varying pressure [35], for a range of different laser operating conditions (irradiance, pulse duration and wavelength) [36], background gases [37] and metal targets [38], but always for a single laser pulse.

Because the model is only one-dimensional, it assumes vapor plume expansion in the forward direction. This is fine for the first (few) 100 ns, but afterwards, the expansion in the radial direction cannot be neglected anymore. Furthermore, the model assumes the plasma to be in LTE conditions, which becomes also questionable for longer simulation times, due to the growing importance of electron–ion recombination upon cooling of the vapor plume. Finally, particle formation by condensation in the expanding (cooling) vapor plume then starts to become important as well. For these reasons, we have applied the model here for only 200 ns, and therefore, the interpulse

delay time was limited to the ns-scale. Although most enhancements for LIBS are reported for interpulse delay times in the (sub) $\mu$ s-scale, we believe that our simulation results can still be useful to obtain more insight in the mechanisms of DP LIBS.

### 3. Results and discussion

The model is applied to DP LIBS in a collinear configuration. Two laser pulses of 266 nm are focused on a copper target in a helium ambient gas of 1 atm. The pulse widths are 5 ns (full-width-half-maximum) and the interpulse delay times are varied between 10 and 100 ns. The laser irradiance of both pulses is equal to  $0.5 \text{ GW/cm}^2$ , yielding a total of  $1 \text{ GW/cm}^2$ . The results will be compared with single pulse (SP) LIBS for a laser irradiance of  $1 \text{ GW/cm}^2$  (same pulse shape, hence same total laser energy).

#### 3.1. Target heating, melting and vaporization

Fig. 1 shows the calculated temperature distributions inside the target material, for SP LIBS (a), and DP LIBS with interpulse delay times of 10 ns (b), 20 ns (c), 50 ns (h) and 100 ns (i). Also the spatial distributions of molten and solid regions in the target are illustrated for these conditions (d, e, f, j, k). Finally, figure (g) presents the detailed surface temperature as a function of time, for all conditions. It is clear that the surface temperature is higher in the SP case, which is logical because the laser irradiance is twice as high (see above). At  $1 \text{ GW/cm}^2$  the surface temperature was calculated to reach a maximum of 7000 K, whereas at  $0.5 \text{ GW/cm}^2$  the maximum surface temperature is in the order of 6000 K. However, in the DP configuration, the surface temperature rises a second time, as a result of the second laser pulse. Consequently, after 200 ns, the surface temperature is higher in the DP

configuration, especially for the longer interpulse delay times (see Fig. 1(g)). As mentioned above, the model is only applied during 200 ns, and for a maximum interpulse delay time of 100 ns, but it is expected that the predicted trend is continued for longer interpulse delay times and plume expansion times as well. As can be seen from Fig. 1(a, b, c, h, i) the temperature distribution plots inside the target look very similar for the SP and various DP configurations.

On the other hand, the distribution of molten and solid phases is quite different, as observed in Fig. 1(d, e, f, j, k). Indeed, in the SP case, the target material is again solidified after 70 ns, but in the DP configurations, the material remains in the molten phase during a longer time, due to the fact that the surface temperature drops more slowly as a function of time.

At interpulse delay times of 50 and especially 100 ns, the target material (almost) solidifies again in between the two pulses (see Fig. 1(j, k)). A similar behavior was reported by De Giacomo et al. [27], who stated that the coupling of the two laser pulses at the target is only effective for an interpulse delay time below a few 100 ns, because for delay times in the order of  $\mu$ s, the target surface has enough time to reach equilibrium [27].

However, for the interpulse delay times of 10 and 20 ns, the material remains in the molten phase, as is clear from Fig. 1(e, f). This observation can have important consequences for the laser ablation process. Indeed, ablation does not only occur by vaporization of the target material, but also by splashing of the molten target [34,39,40]. This process is not yet taken into account in our model, but qualitatively we can predict that this mechanism of laser ablation will become more important in the DP configuration, and hence, that the overall amount of laser ablation will be enhanced in comparison to the SP configuration. Such enhanced laser ablation (or mass removal rate) is also experimentally observed by Forsman et al. [29] for laser

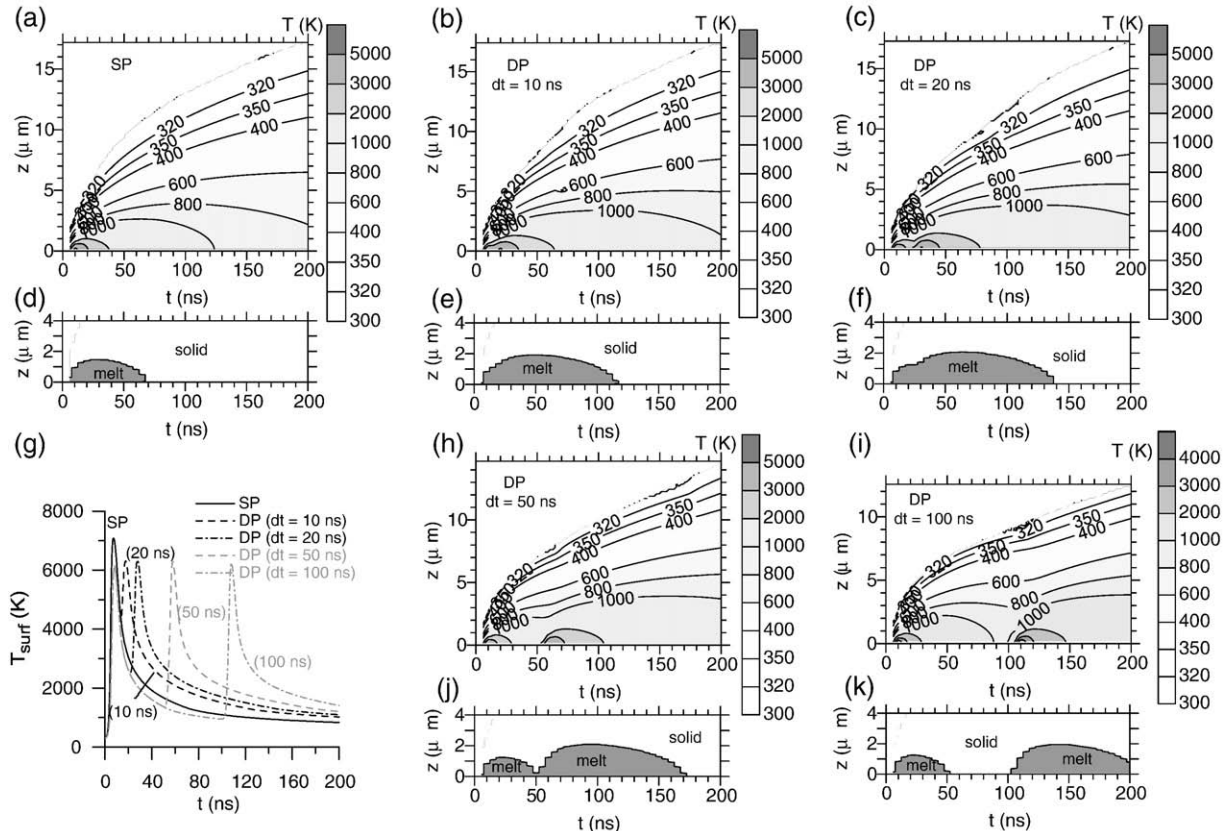


Fig. 1. Temperature distributions inside the copper target as a function of time, for the SP configuration (a) and the DP configurations with interpulse delay times of 10 ns (b), 20 ns (c), 50 ns (h) and 100 ns (i), as well as the corresponding melt distributions inside the target as a function of time, for the SP configuration (d) and the DP configurations with interpulse delay times of 10 ns (e), 20 ns (f), 50 ns (j) and 100 ns (k). Also shown is the surface temperature as a function of time for the SP and the different DP configurations (g).

ablation of metals (aluminum, steel) in air, at similar laser operating conditions (i.e., interpulse delay times of 30–150 ns).

In Ref. [18] the laser ablation depth was found to be larger for the DP case than for the SP case, and the crater rims were less obvious. This was attributed to a lower amount of resolidification of the molten material (and hence to a lower amount of melting). The latter is in contradiction with our model predictions. However, the interpretation of Ref. [18] was not necessarily true, as Forsman attributed the reduced crater rim formation to the fact that the created debris were used by the second laser pulse (see Introduction) [29].

As illustrated in Fig. 2, the amount of laser vaporization is calculated to be somewhat lower in the DP configuration, which is attributed to the lower surface temperature. Indeed, the amount of vaporization in the model is directly proportional to the surface temperature, through the Clausius–Clapeyron equation [34]. Even after the second pulse, the evaporation depth remains slightly lower compared to the SP configuration. However, if we compare the calculated evaporation depths ( $\sim 40$  nm) with the calculated melt depths ( $\sim 2$   $\mu\text{m}$ ), it can be argued that laser ablation due to liquid splashing has probably a larger contribution than vaporization, to the total amount of target mass ablation. Similar conclusions were made

in Ref. [38] for different metals, where it was demonstrated that the calculated evaporation and melt depths are lower and upper bounds for the actual, measured crater depths, respectively, and the relative role of vaporization and melt expulsion was found to be different for different metals [38]. For instance, melt expulsion was predicted to be much more important for aluminum than for iron, so one could expect that the enhancement in the mass removal rate in the DP configuration compared to the SP case will be higher for aluminum than for iron. In Ref. [9] it is indeed reported that the DP configuration is more effective for aluminum than for steel, so the above mechanism could be one of the explanations for it.

On the other hand, it might also be possible that melt splashing becomes less pronounced in the DP case, because it results typically from the plasma recoil pressure and the background gas pressure is reduced in the DP configuration. In that case, phase explosion might be responsible for larger craters and signal enhancements observed in the DP case. In future work, we hope to be able to include both melt splashing and phase explosion in our model.

### 3.2. Laser absorption in the plasma

Fig. 3 presents the laser irradiance temporal profiles in the case of the SP configuration (a) and the DP configurations, with interpulse delay times of 10 ns (b), 20 ns (c), 50 ns (d) and 100 ns (e). Beside the original laser profiles (solid lines), also the laser irradiance arriving at the target is plotted (dashed lines). It is clear that a considerable fraction of the laser irradiance is absorbed by the vapor plasma in front of the target, especially in the case of the SP configuration, where the laser irradiance was 1 GW/cm<sup>2</sup>. Indeed, almost 50% of the laser energy appears to be absorbed in the plasma, as a result of electron-neutral and electron-ion inverse Bremsstrahlung. A similar result was also found in our earlier simulations [36].

In the DP configuration, the amount of plasma absorption during the first pulse is much lower, because of the lower laser irradiance. This is again in accordance with our previous calculation results [34,36], and is explained by the lower vapor density, plume temperature and ionization degree in the plasma, at lower laser irradiance. However, during the second laser pulse, there is more energy absorption in the plasma, at least for the smaller interpulse delay times (see Fig. 3(b, c)). Indeed, at such short delay times, the plasma originating from the first laser pulse is still hot, and participates in the plasma shielding, when the second laser pulse is focused on the target. This was also discussed by Russo et al. [14]. For longer laser interpulse delay times, the influence of the first plasma becomes gradually less important (see Fig. 3(d, e)).

Integrated over the two laser pulses, the amount of plasma absorption was found to be considerably lower in the DP configuration, compared to the SP case, and decreases also with increasing interpulse delay times (see Fig. 3(b–e)). If we extrapolate this behavior to interpulse delay times in the  $\mu\text{s}$ -range, which are more typically used in DP LIBS, and where the influence of the first laser pulse plasma will become negligible, it is expected indeed that the amount of plasma absorption is considerably lower in the DP configuration. Hence, more laser energy will become available for the target laser ablation process itself. This was indeed demonstrated by Russo et al. for interpulse delay times larger than 200 ns [14]. As mentioned in the Introduction section, several authors reported less effective shielding of the second laser pulse. However, this was typically obtained for laser interpulse delay times in the  $\mu\text{s}$ -range, where the effect of the first laser plasma was completely negligible, and where the effect of ambient gas reduction was significant [4–7,9,11,16–19].

### 3.3. Plume expansion dynamics and plasma formation

In Figs. 4 and 5, the plume expansion process is visualized, for the SP and the DP configuration, respectively. Only the results for an

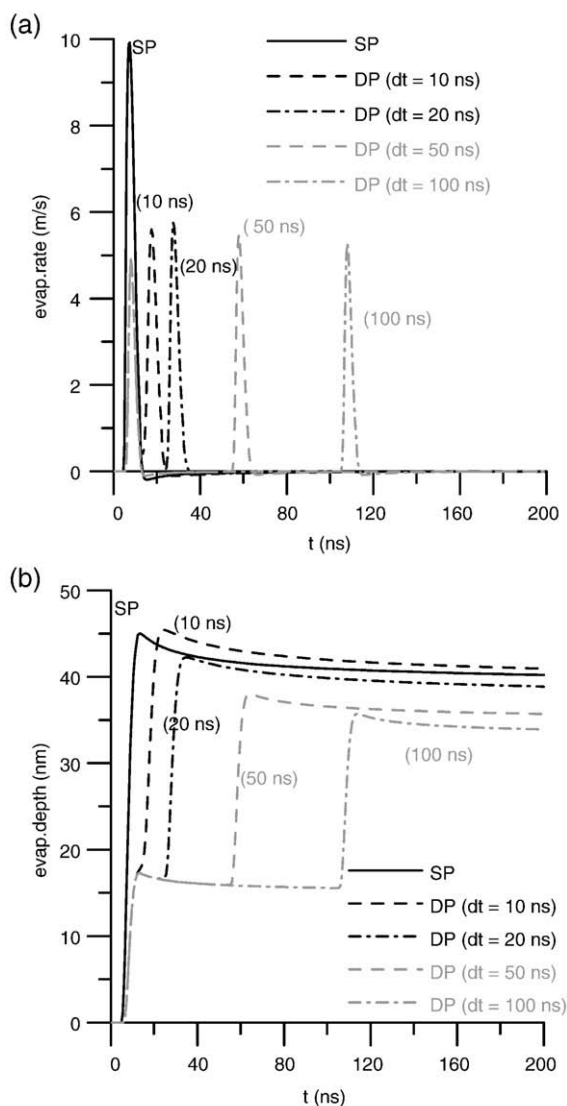
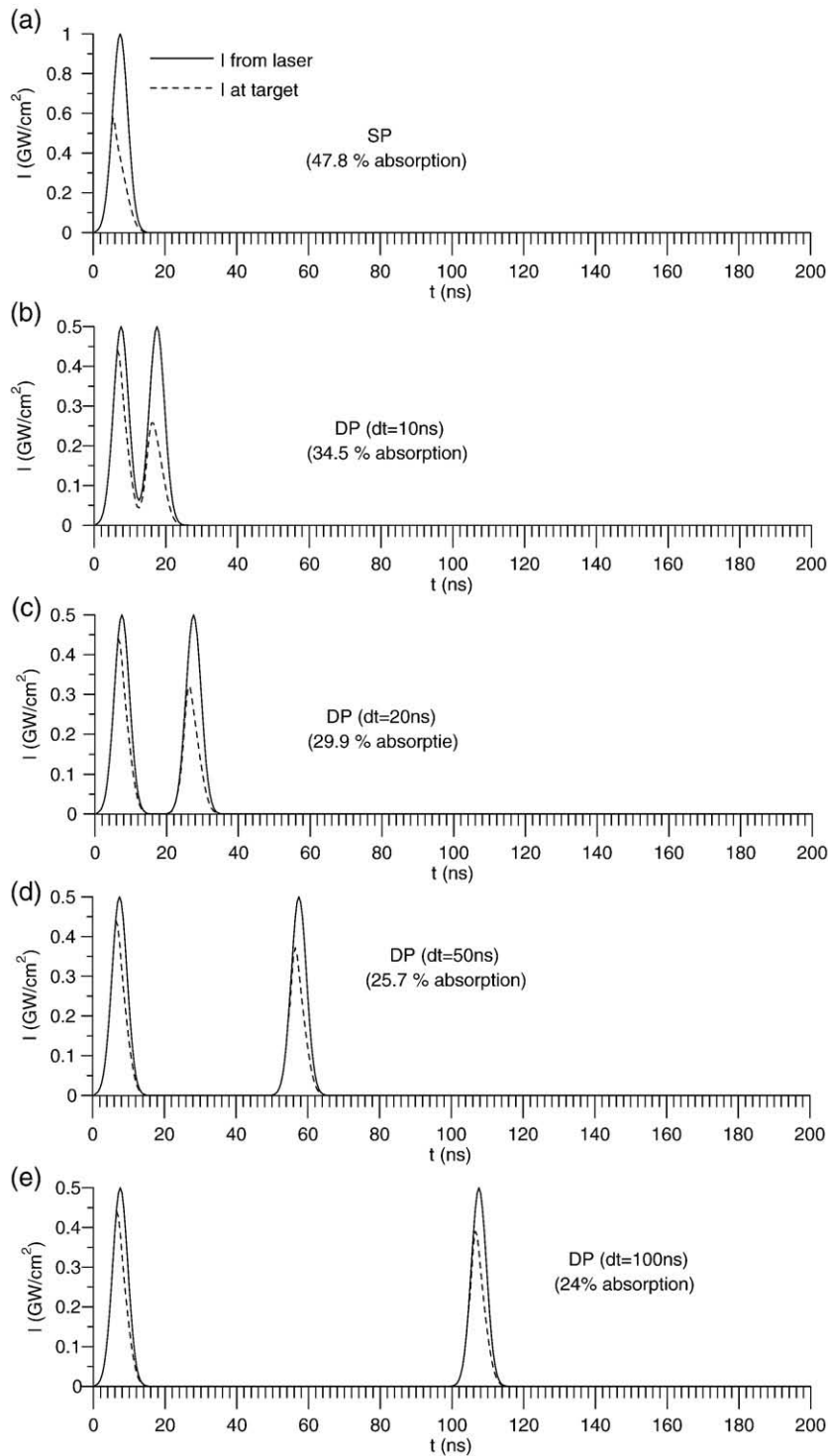


Fig. 2. Evaporation rates (a) and evaporation depths (b) for the SP and the different DP configurations.



**Fig. 3.** Laser irradiance originating from the laser (solid lines) and arriving at the target after passing through the plasma (dashed lines), for the SP configuration (a), and the DP configurations with interpulse delay times of 10 ns (b), 20 ns (c), 50 ns (d) and 100 ns (e). The percentage of plasma absorption is indicated in each case.

interpulse delay time of 50 ns are illustrated, but the other DP delay times gave qualitatively very similar results. In the SP configuration (Fig. 4), the vapor plume expands against the background gas. This results in a gradual drop of the vapor density (Fig. 4(a)), because it is more spread out. At the same time, the background gas is pushed away from the target, and is piled up at the end of the vapor plume (Fig. 4(b)). Note that the gas density value of  $2.45 \times 10^{25} \text{ m}^{-3}$  corresponds to the undisturbed background gas density at 1 atm and 300 K. The plume velocity is calculated in the order of 8000–

10,000 m/s (Fig. 4(c)), and the plume temperature ranges from 10,000 till 40,000 K (Fig. 4(d)), which is in accordance to our previous calculation results for the same conditions [33,36]. The electron density (Fig. 4(e)) has a very similar profile as the vapor density profiles.

In the DP configuration, the vapor plume expansion looks qualitatively very similar, as is apparent from Fig. 5. However, the plume dimensions are somewhat smaller (see Fig. 5(a, b)), because the amount of vaporization and the maximum surface temperature are

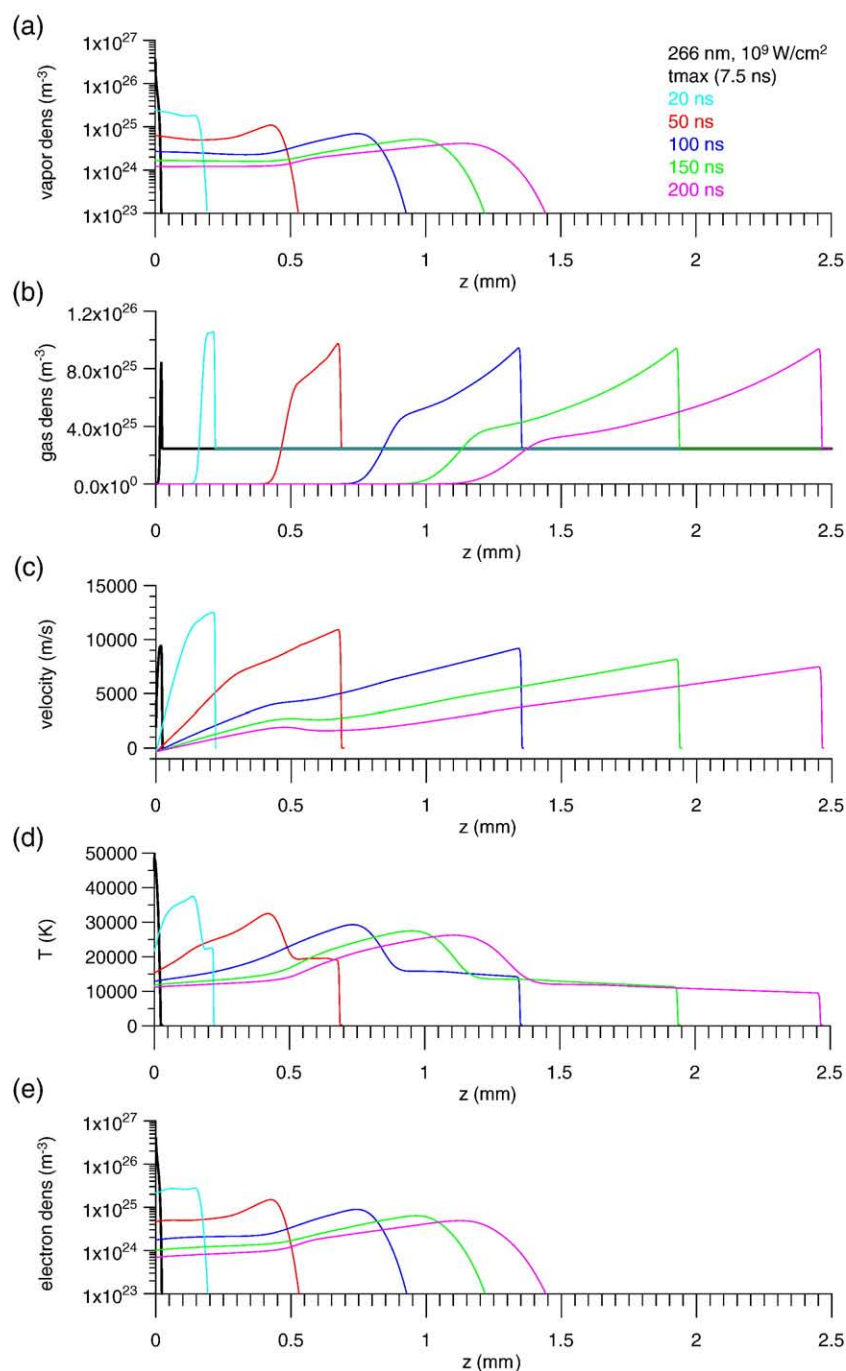


Fig. 4. Vapor density (a), background gas density (b), plume velocity (c) and temperature (d) and electron density in the plasma (e), at different times, for the SP configuration.

lower (due to the lower laser irradiance of one pulse, see above) and consequently, the vapor plume velocity is smaller (see Fig. 5(c)).

On the other hand, it is clearly seen from Fig. 5(c) that the plume velocity distribution at 100 and 150 ns (i.e., after the second laser pulse) is characterized by two peaks, i.e., the first peak due to the first laser pulse, and the second peak (i.e., still closer to the target) resulting from the second laser pulse. Moreover, the second velocity peak is higher, which is the consequence of the background gas reduction as a result of the first laser peak (see Fig. 5(b)). At 200 ns, the plume velocity still has two peaks, but the first velocity peak is almost caught up by the second (i.e., higher) velocity peak. This behavior is in good correlation with the simulation results reported by De Giacomo et al.

[27]. Indeed, the shock wave produced by the second laser pulse travels faster and eventually merges with the first shock wave [27].

At first sight, the smaller plume dimensions are in contradiction to the observations made in the literature, where most often larger plasma volumes are observed (e.g., [6,7,11,14]). However, in the mentioned studies, the laser interpulse delay time was typically in the  $\mu\text{s}$ -range, and the effect of background gas reduction was found to be very significant. Our simulations also predict that the background gas is pushed away from the target, and hence that there is gas rarefaction in front of the target (see Fig. 5(b)). This results indeed in a faster plume expansion, as is observed in the velocity profiles of Fig. 5 (c), where the second velocity peak in the curves at 100, 150 and

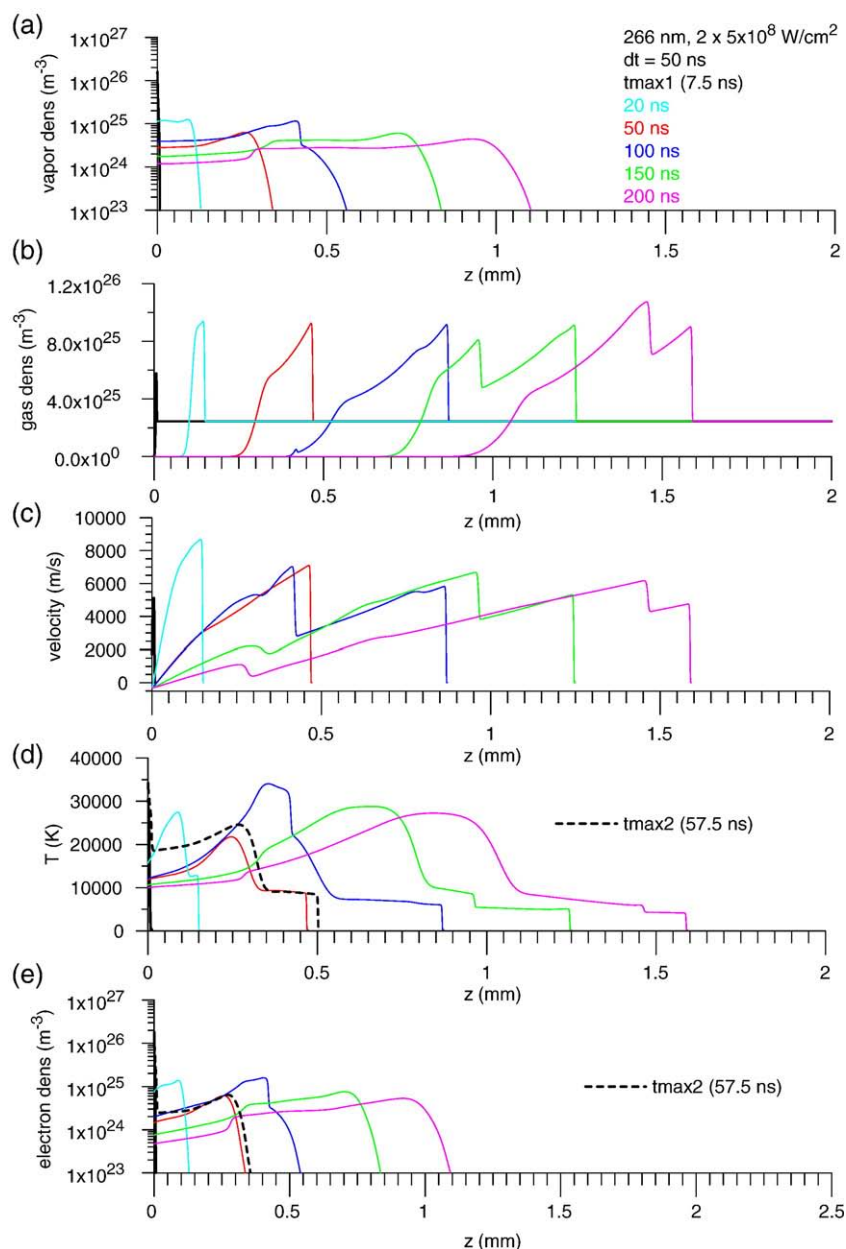


**Fig. 5.** Vapor density (a), background gas density (b), plume velocity (c) and temperature (d) and electron density in the plasma (e), at different times, for the DP configuration with interpulse delay time of 50 ns. The results at the maximum of the first laser pulse are presented with a thicker line, to clearly visualize their behavior near the target. The plume temperature and electron density in the plasma are also shown at the maximum of the second laser pulse (i.e., 57.5 ns) (see thick dashed lines in figure (d) and (e)), to illustrate that they both rise again, especially near the target.

200 ns is higher than the first velocity peak (see discussion above). Moreover, our calculations predict in general indeed a faster expansion when the background gas pressure in front of the target is lower, as was clearly demonstrated in Ref. [35]. Hence, this effect applies also to the present simulations, but apparently, it is compensated by the lower laser irradiance of one peak in the DP configuration (which is only half of the laser irradiance in the SP case), giving rise to a lower amount of vaporization and therefore a lower plume velocity (see discussion above). Note that, if we would have assumed the same laser irradiance for both laser pulses in the DP case as in the SP configuration (hence: total laser energy of the DP case is then twice the laser energy of the SP case, like in Ref. [27]), we would also have obtained larger plume dimensions in the DP configuration.

The temperature distributions in the plume are plotted in Fig. 5(d). At a time of 20 and 50 ns, the plume temperature has dropped

significantly compared to the value at 7.5 ns, which is at the peak of the first laser pulse. Indeed, during the laser pulse, a considerable fraction of the laser energy is absorbed by the plasma, leading to a high plasma temperature. After the laser pulse, the temperature drops down slowly as a result of the plume expansion. However, at 57.5 ns (see thicker dashed curve in Fig. 5(d)), the plasma temperature has again increased dramatically compared to the value at 50 ns, due to the laser absorption of the second laser pulse. Note that the value at 100 ns is very high too, which is a direct result of the second laser pulse. In fact, the vapor density was also somewhat higher at 100 ns (see Fig. 5(a)), compared to the trend observed in the SP configuration (Fig. 4(a)). The same effect is clearly visible for the electron density as well (see Fig. 5(e)), where the result at 57.5 ns (thicker dashed curve) is again characterized by a high electron density near the target, and the electron density at 100 ns is also still higher than the values at, for

instance, 50 ns (i.e., before the second laser pulse). The higher electron density is of course a direct consequence of the higher plasma temperature, which yields a higher ionization degree according to the LTE assumption (Saha equations) [34].

Fig. 6 shows in detail this effect of the second laser pulse on the plasma temperature and electron density, at the maximum of their profile, not only for the DP configuration with 50 ns delay time, but also for the other interpulse delay times investigated, as well as for the SP configuration. In the SP configuration, the maximum plasma temperature and electron density drop gradually as a function of time. In the DP configuration, on the other hand, the initial maximum plasma temperature and electron density are lower due to the lower laser irradiance, but they increase upon arrival of the second laser pulse, after which they decrease again. However, at 200 ns, the maximum plasma temperature and electron density are still found to be slightly higher than in the SP configuration, especially for the longer interpulse delay times.

Experimentally, some authors observed an increase in the plasma temperature and electron density in the DP configuration [4,8,12,31], but the effect was not always so significant [4,11], and was sometimes even observed to be opposite [6,14], possibly attributed to the faster plume expansion [14]. Our simulations show that the enhancements in plasma temperature and electron density depend strongly on the

time of observation, i.e., shortly enough after the second laser pulse, enhancements are predicted by our model, but after some time, the differences have become negligible. This might explain why some authors observe enhancements and others do not.

#### 4. Conclusion

A model describing laser–target interaction (i.e., heating, melting and vaporization), as well as vapor plume expansion, plasma formation and laser–plasma interaction, is used to investigate the effects of DP LIBS, in the case of laser ablation of copper in a helium ambient gas at 1 atm. Because of the one-dimensional character of the model, it can only produce realistic calculation results until about 200 ns. Therefore, the interpulse delay times were varied between 10 and 100 ns. Comparison was made with calculation results for the SP LIBS configuration at the same total laser energy.

It is found that the maximum surface temperature of the copper target is slightly lower in the DP configuration, due to the lower laser irradiance of one pulse, and this results in a somewhat lower amount of target evaporation. On the other hand, the surface temperature rises again upon the second laser pulse, and it remains somewhat higher at longer observation times (i.e., 200 ns). As a result of this, the copper target remains in molten phase for a longer time in the DP configuration, which might have the consequence of more laser ablation due to liquid splashing of the molten target.

The laser absorption in the plasma is found to be considerably lower in the DP configuration (i.e., in the range of 24–34% compared to 48% for the SP case). Moreover, it becomes lower for longer interpulse delay times. We expect that this trend is continued also for delay times in the  $\mu\text{s}$ -range, where the effect of the first laser plasma becomes even more negligible. This lower amount of plasma shielding means that relatively more laser energy will be available for the laser ablation process itself in the DP configuration.

Furthermore, the plume expansion dynamics clearly demonstrate two separate waves of plume expansion (as observed in the plume velocity profiles), as a result of the two laser pulses in the DP configuration. The second velocity peak (i.e., resulting from the second laser pulse) is higher than the first velocity peak. This is attributed to the reduced background gas pressure in front of the target, as the background gas is already pushed away from the target as a result of the first laser pulse. Moreover, the maximum plasma temperature and electron density, although initially lower than in the SP case, increase again upon the second laser pulse, and consequently they are still somewhat higher than in the SP configuration after e.g., 200 ns.

Our calculation results have been compared with experimental data, whenever possible. Although most experimental data are reported for longer observation times and longer interpulse delay times (typically in the  $\mu\text{s}$ -range), our model predictions can still be useful to explain the trends in the experimental observations.

#### Acknowledgments

A. Bogaerts wishes to thank N. Omenetto for the interesting discussions. The authors acknowledge financial support from the Fund for Scientific Research (FWO) – Flanders, the IAP-VI project, and the CALCUA computing facilities of the University of Antwerp.

#### References

- [1] L.J. Radziemski, D.A. Cremers, *Laser-induced Plasmas and Applications*, Marcel Dekker, New York 1989.
- [2] J.D. Winefordner, I.B. Gornushkin, T. Correll, E. Gibb, B.W. Smith, N. Omenetto, Comparing several atomic spectrometric methods to the super stars: special emphasis on laser induced breakdown spectrometry, LIBS, a future super star, *J. Anal. At. Spectrom.* 19 (2004) 1061–1083.
- [3] V.I. Babushok, F.C. DeLucia Jr., J.L. Gottfried, C.A. Munson, A.W. Miziolek, Double pulse laser ablation and plasma: laser induced breakdown spectroscopy signal enhancement, *Spectrochim. Acta Part B* 61 (2006) 999–1014.

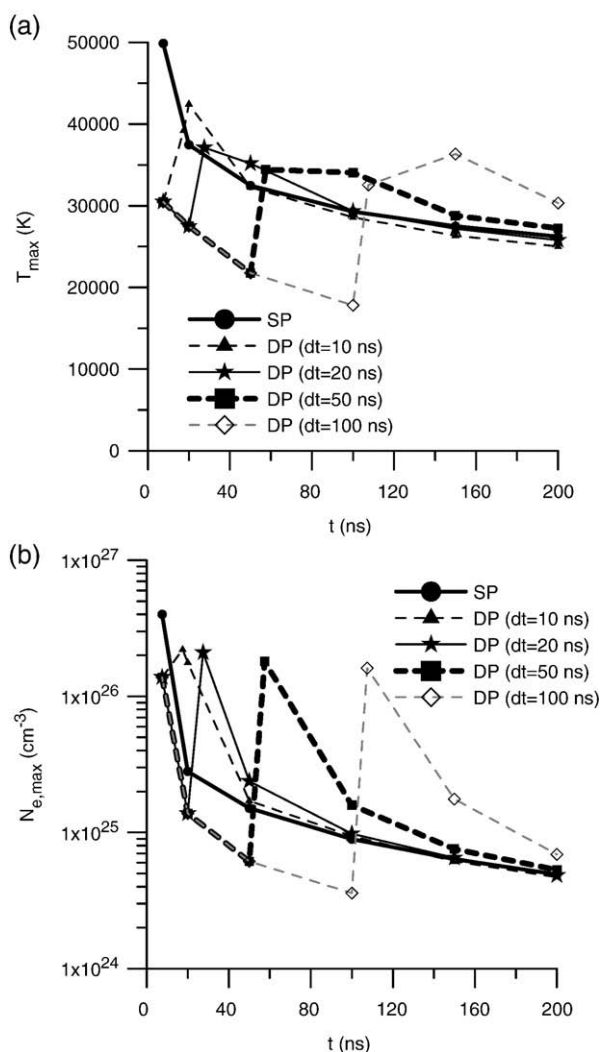


Fig. 6. Maximum plasma temperature (a) and electron density in the plasma (b) as a function of time, for the SP and the different DP configurations. The results for an interpulse delay time of 50 ns are plotted in thicker line, to clearly illustrate the rise in temperature and electron density as a result of the second pulse.

- [4] P.A. Benedetti, G. Cristoforetti, S. Legnaioli, V. Palleschi, L. Pardini, A. Salvetti, E. Tognoni, Effect of laser pulse energies in laser induced breakdown spectroscopy in double-pulse configuration, *Spectrochim. Acta Part B* 60 (2005) 1392–1401.
- [5] G. Cristoforetti, S. Legnaioli, V. Palleschi, A. Salvetti, E. Tognoni, Influence of ambient gas pressure on laser-induced breakdown spectroscopy technique in the parallel double-pulse configuration, *Spectrochim. Acta Part B* 59 (2004) 1907–1917.
- [6] M. Corsi, G. Cristoforetti, M. Giuffrida, M. Hidalgo, S. Legnaioli, V. Palleschi, A. Salvetti, E. Tognoni, C. Vallebona, Three-dimensional analysis of laser induced plasmas in single and double pulse configuration, *Spectrochim. Acta Part B* 59 (2004) 723–735.
- [7] G. Cristoforetti, S. Legnaioli, V. Palleschi, A. Salvetti, E. Tognoni, Characterization of a collinear double pulse laser-induced plasma at several ambient gas pressures by spectrally- and time-resolved imaging, *Appl. Phys. B* 80 (2005) 559–568.
- [8] L. St-Onge, V. Detalle, M. Sabsabi, Enhanced laser-induced breakdown spectroscopy using the combination of fourth-harmonic and fundamental Nd:YAG laser pulses, *Spectrochim. Acta Part B* 57 (2002) 121–135.
- [9] C. Gautier, P. Fichet, D. Menut, J. Dubessy, Applications of the double-pulse laser-induced breakdown spectroscopy (LIBS) in the collinear beam geometry to the elemental analysis of different materials, *Spectrochim. Acta Part B* 61 (2006) 210–219.
- [10] C. Gautier, P. Fichet, D. Menut, J.-L. Lacour, D. L'Hermite, J. Dubessy, Main parameters influencing the double-pulse laser-induced breakdown spectroscopy in the collinear beam geometry, *Spectrochim. Acta Part B* 60 (2005) 792–804.
- [11] R. Noll, R. Sattmann, V. Sturm, S. Winkelmann, Space- and time-resolved dynamics of plasmas generated by laser double pulses interacting with metallic samples, *J. Anal. At. Spectrom.* 19 (2004) 419–428.
- [12] R. Sattmann, V. Sturm, R. Noll, Laser-induced breakdown spectroscopy of steel samples using multiple Q-switch Nd:YAG laser pulses, *J. Phys. D: Appl. Phys.* 28 (1995) 2181–2187.
- [13] F. Colao, V. Lazic, R. Fantoni, S. Pershin, A comparison of single and double pulse laser-induced breakdown spectroscopy of aluminum samples, *Spectrochim. Acta Part B* 57 (2002) 1167–1179.
- [14] X. Mao, X. Zeng, S.-B. Wen, R.E. Russo, Time-resolved plasma properties for double pulsed laser-induced breakdown spectroscopy of silicon, *Spectrochim. Acta Part B* 60 (2005) 960–967.
- [15] A. Casavola, A. De Giacomo, M. Dell'Aglio, F. Taccogna, G. Colonna, O. De Pascale, S. Longo, Experimental investigation and modelling of double pulse laser induced plasma spectroscopy under water, *Spectrochim. Acta Part B* 60 (2005) 975–985.
- [16] A. De Giacomo, M. Dell'Aglio, O. De Pascale, M. Capitelli, From single pulse to double pulse ns-laser induced breakdown spectroscopy under water: elemental analysis of aqueous solutions and submerged solid samples, *Spectrochim. Acta Part B* 62 (2007) 721–738.
- [17] V. Burakov, N. Tarasenko, M. Nedelko, S. Isakov, Time-resolved spectroscopy and imaging diagnostics of single pulse and collinear double pulse laser induced plasma from a glass sample, *Spectrochim. Acta Part B* 63 (2008) 19–26.
- [18] L. Caneve, F. Co, I. a o, R. Fantoni, V. Spizzichino, Laser ablation of copper based alloys by single and double pulse laser induced breakdown spectroscopy, *Appl. Phys. A* 85 (2006) 151–157.
- [19] G. Cristoforetti, S. Legnaioli, L. Pardini, V. Palleschi, A. Salvetti, E. Tognoni, Spectroscopic and shadowgraphic analysis of laser induced plasmas in the orthogonal double pulse pre-ablation configuration, *Spectrochim. Acta Part B* 61 (2006) 340–350.
- [20] S.M. Angel, D.N. Stratis, K.L. E, la nd, T. Lai, M.A. Berg, D.M. Gold, LIBS using dual- and ultra-short laser pulses, *Fresenius J. Anal. Chem.* 369 (2001) 320–327.
- [21] V. Hohreiter, D.W. Hahn, Dual-pulse laser induced breakdown spectroscopy: time-resolved transmission and spectral measurements, *Spectrochim. Acta Part B* 60 (2005) 968–974.
- [22] D.N. Stratis, K.L. E, land, S.M. Angel, Dual-pulse LIBS using a pre-ablation spark for enhanced ablation and emission, *Appl. Spectrosc.* 54 (2000) 1270–1274.
- [23] A. Kuwako, Y. Uchida, K. Maeda, Supersensitive detection of sodium in water with use of dual-pulse laser-induced breakdown spectroscopy, *Appl. Optics* 42 (2003) 6052–6056.
- [24] J. Scaffidi, J. Pender, W. Pearman, S.R. Goode, B.W. Colston Jr., J.C. Varter, S.M. Angel, Dual-pulse laser-induced breakdown spectroscopy with combinations of femto-second and nanosecond laser pulses, *Appl. Optics* 42 (2003) 6492–6499.
- [25] J. Scaffidi, S.M. Angel, D.A. Cremers, Emission enhancement mechanisms in dual-pulse LIBS, *Anal. Chem.* 78 (2006) 25–32.
- [26] E. Tognoni, G. Cristoforetti, S. Legnaioli, V. Palleschi, N. Omenetto, I. Gornushkin, Spectroscopic Study of the Factors Concurring to Intensity Enhancement in Double Pulse LIBS, Poster Presentation at the Euro-Mediterranean Symposium on Laser-induced Breakdown Spectroscopy, Paris, September 10–13, 2007.
- [27] A. De Giacomo, M. Dell'Aglio, D. Bruno, R. Gaudioso, O. De Pascale, Experimental and theoretical comparison of single-pulse and double-pulse LIBS on metallic samples, *Spectrochim. Acta Part B* 63 (2008).
- [28] J. Gonzalez, C. Liu, J. Yoo, X. Mao, R.E. Russo, Double-pulse laser ablation inductively coupled plasma mass spectrometry, *Spectrochim. Acta Part B* 60 (2005) 27–31.
- [29] A.C. Forsman, P.S. Banks, M.D. Perry, E.M. Campbell, A.L. Dodell, M.S. Armas, Double-pulse machining as a technique for the enhancement of material removal rates in laser machining of metals, *J. Appl. Phys.* 98 (2005) 033302.
- [30] J. Zhang, K. Sugioka, S. Wada, H. Tashiro, K. Toyoda, Dual-beam ablation of fused quartz using 266 nm and VUV lasers with different delay-times, *Appl. Phys. A* 64 (1997) 477–481.
- [31] P. Mukherjee, S. Chen, S. Witanachchi, Effect of initial plasma geometry and temperature on dynamic plume expansion in dual-laser ablation, *Appl. Phys. Lett.* 74 (1999) 1546–1548.
- [32] A. Semerok, C. Dutouquet, Ultrashort double pulse laser ablation of metals, *Thin Solid Films* 453–454 (2004) 501–505.
- [33] Z. Chen, A. Bogaerts, Laser ablation of Cu and plume expansion into 1 atm ambient gas, *J. Appl. Phys.* 97 (2005) 063305.
- [34] A. Bogaerts, Z. Chen, R. Gijbels, A. Vertes, Laser ablation for analytical sampling: what can we learn from modeling? *Spectrochim. Acta Part B* 58 (2003) 1867–1893.
- [35] Z. Chen, D. Bleiner, A. Bogaerts, Effect of ambient pressure on laser ablation and plume expansion dynamics: a numerical simulation, *J. Appl. Phys.* 99 (2006) 063304.
- [36] A. Bogaerts, Z. Chen, Effect of laser parameters on laser ablation and laser-induced plasma formation: a numerical modelling investigation, *Spectrochim. Acta Part B* 60 (2005) 1280–1307.
- [37] A. Bogaerts, Z. Chen, D. Bleiner, Laser ablation of copper in different background gases: comparative study by numerical modeling and experiments, *J. Anal. At. Spectrom.* 21 (2006) 384–395.
- [38] D. Bleiner, Z. Chen, D. Autrique, A. Bogaerts, Role of laser-induced melting and vaporization of metals during ICP-MS and LIBS analysis, investigated by computer simulations and experiments, *J. Anal. At. Spectrom.* 21 (2006) 910–921.
- [39] L.V. Zhigilei, Dynamics of the plume formation and parameters of the ejected clusters in short-pulse laser ablation, *Appl. Phys. A* 76 (2003) 339–350.
- [40] A.A. Oraevsky, S.L. Jacques, F.K. Tittel, Mechanisms of laser ablation for aqueous media irradiated under confined-stress conditions, *J. Appl. Phys.* 78 (1995) 1281–1290.